JOURNAL OF MATERIALS SCIENCE **37** (2002) 2659–2667

Characterization of microstructures and toughening behavior of fiber-containing toughened nylon 6,6

S. C. WONG*,§, G. X. SUI‡, C. Y. YUE‡
*Schools of *Materials Engineering and ‡Mechanical and Production Engineering, Nanyang Technological University, Nanyang Avenue, Singapore 639798, Republic of Singapore*
E-mail: asscwong@ntu.edu.sg

Y.-W. MAI
Center for Advanced Materials Technology (CAMT), School of Aerospace, Mechanical and Mechatronic Engineering, The University of Sydney, Sydney, NSW 2006, Australia, MEEM, City University of Hong Kong, Tat Chee Avenue, Kowloon, Hong Kong, People's Republic of China

The toughening behavior of short glass fiber reinforced toughened polymers was studied using fracture mechanics and microscopic techniques. The essential work of fracture (EWF) analysis shows that the inclusion of short glass fibers not only provided a stiffening effect but also a toughening influence. It was observed that rubber-related toughening and fiber-related toughening were competitive in nature for the reinforced, toughened nylon 6,6. When the matrix stress was substantially reduced by the presence of short fibers via the load-shedding mechanism, rubber toughening was severely curtailed. At higher fiber volume fractions, fiber pull-out work contributed significantly to the enhancement of the specific essential fracture work. Fiber-end plasticity was evident under microscopic examination.

1. Introduction

Toughening of engineering polymers using second elastomeric phase has found wide-ranging applications in the automotive and packaging industries. The attempt to elucidate the toughening mechanisms has also accomplished considerable success [1–3]. In recent years, there has been an increased interest in introducing high modulus glass fibers [4–9] and glass beads [10–12] into toughened matrices. One clear advantage of such a design scheme is the cost-effective fabrication; and the primary motivation is to reinforce the toughened matrix, which often suffers from reduction in tensile strength and modulus caused by the compliant rubber particles. The ideal scenario appears to be one that can accomplish concomitantly toughening as derived from the matrix and strengthening as derived from the reinforcement. This scenario often does not hold because of the complexity in interaction between the impact modifiers and the reinforcement. Some success in obtaining high strength and high toughness blends with glass fiber reinforcements was, nevertheless, reported [7, 8, 13]. The toughness in this case was defined as the work dissipated per unit area of crack growth.

The theories of rubber toughening were well studied and reviewed by Bucknall in Chapter 22 of Ref. [3]. It arises when matrix plasticity was promoted by internal cavitation of rubber particles or by adhesive failure at the particle-matrix boundary. It is noteworthy that for rubber particles that do not serve the purpose of enhancing matrix deformation, which absorbs the predominant amount of energy, there is no reason for rubber toughening. In such cases, the compliant rubber particles only serve to weaken the matrix material and lead to lower toughness.

Recent attention has been given to characterizing mechanical and fracture properties of fiber-reinforced toughened polymers using fracture mechanics [4–9, 14, 15]. However, toughening mechanisms of fiber-reinforced toughened plastics are not very well understood particularly with regard to the independent roles of second phases and their interactions [3, 13, 16]. One would conjecture that the mechanisms of fracture in connection with fiber-reinforced single polymers [14] could be applied to reinforced, toughened polymers. This approach ignores the distinctive role of the second-phase rubber particles and assumes the rubber-toughened matrix to possess certain effective properties in the presence of glass fibers. The actual fracture events as to whether there is a need for both fibers and rubbery phase to be present for toughening remain unclear. It is understood that the presence of fibers reduces the stress borne by the matrix material, being

§Author to whom all correspondence should be addressed.

controlled by their relative stiffness and fiber volume fraction. The interesting question is whether toughening can still be effected with elastomeric inclusions under such circumstances. There appears to be a transition from matrix-dominant mechanisms to fiber-related mechanisms such as fiber debonding, fiber bridging and fiber pullout when the matrix-borne stress is severely curtailed. However, the fibers could also induce matrix plasticity due to fiber-end debonding. In this paper, we study the microstructure and identify the role of fibers on toughened nylon 6,6. Techniques using optical and electron microscopy were employed to study the morphology and crack-tip deformation mechanisms.

2. Experimental work

2.1. Materials

The polymer used in this work was rubber-toughened nylon 6,6 (Zytel ST801), which contained 20 vol% EPDM rubber [3], from DuPont (Singapore) Pte. Ltd. The glass fibers were chopped E-glass fibers with a mean diameter of 17 μm and a length of 12 mm. Materials were compounded simultaneously at weight ratios of 0, 10, 20, 30 and 40 wt% of short glass fibers in the toughened nylon 6,6 matrix. All materials were dry blended and compounded using a co-rotating, intermeshing twin-screw extruder (Leistritz Micro18; screw diameter = 18 mm; $L/D = 30$) at a temperature ranging from 280 to 300°C. The pelletized extrudates were injection molded at around 280°C at relatively high injection speed and injection pressure to form 3.5 mm thick dog-bone specimens (ASTM D638M). Pellets were dried at 80°C for at least 48 h in a vacuum oven prior to compounding and injection molding. Table I shows the equivalent fiber volume fraction taking into account the densities of components for each of the blend compositions. Table II details all the mechanical properties measured after processing. For convenience of discussion, we refer to the weight fraction of the fiber content throughout this paper unless otherwise specified.

2.2. Characterization of microstructures

The injection-molded specimen was cut and embedded in epoxy resin with the viewed surface parallel to the mold filling direction (MFD). This epoxy block was ground and polished to the middle section through the thickness. Photomicrographs were taken using a reflective light microscope (ROM) to show the fiber orientation and fiber distribution. The fiber orientation in comparison to the MFD was analyzed on the photomicrograph using an image analysis software (Image-Pro Plus, Media Cybernetics, L.P.).

To measure the fiber lengths after processing, glass fibers were separated by burning off the polymer matrix of a representative sample of the injection-molded bar and then dispersed on a glass slide for observation under a light microscope. Fiber length distribution was analyzed on the optical micrograph.

Representative injection molded specimens were embedded in epoxy and finely polished followed by staining with vapor from 1% OsO_4 aqueous solution for 24 h. The back-scattered electron images (BEI) were then obtained under the scanning electron microscope (SEM) to characterize the EPDM rubbery phase in an injection-molded bar.

TABLE I Conversion of fiber volume fraction from weight fraction of short glass fiber reinforced toughened nylon 6,6

Fiber weight fraction (wt%)	0	10	20	30	40
Fiber volume fraction (vol%)	0	4.43	9.41	15.18	21.80

TABLE II Mechanical properties of short glass fiber reinforced toughened nylon 6,6

Fiber content (wt%)	0	10	20	30	40
Tensile strength (MPa)	42.71	41.08	53.88	75.16	90.23
Tensile modulus (GPa)	1.83	2.24	3.48	5.46	7.74
Average fiber aspect ratio	NA	~13	~13	~13	~13

2.3. Assessment of fracture toughness

Fracture toughness of the fiber-containing composites was assessed using the essential work of fracture (EWF) approach. Single-edge-notch-bend (SENB) specimens were used for EWF tests. The specimen dimensions were $3.5 \times 10 \times 60$ (mm) and ligaments of different lengths were prepared by a V-notching machine, followed by inserting a fresh razor blade into the notch to make a sharp crack. The final crack-to-width ratios, a/W, were controlled within the range of 0.15–0.80. Three-point bending tests were carried out in an Instron 5569 testing machine with a span of 40 mm and a crosshead speed of 5 mm/min at room temperature.

2.4. Characterization of toughening behavior

Sub-fracture surface and the crack-tip deformation zone were studied using both SEM and optical microscopy. A sub-critical crack was created using a single-edge-double-notch 4-point-bend (SEDN-4-PB) technique [17]. The damage zone ahead of the survived crack-tip was then studied by petrographic thin-sectioning technique under ROM and transmitted optical microscopy (TOM) [17–19].

3. Results and discussions

3.1. Microstructures

The microstructures of fiber-reinforced toughened polymers are complex because they consist of two second-phase fillers in a polymer matrix. Components form interface/interphase between fiber and polymer, polymer and second-phase rubber, and between fiber and second-phase rubber. To reveal the microstructures and fiber distributions for fiber-reinforced toughened polymers, we polished the specimen cross-sections with different fiber volume fractions for SEM examination to be followed by image analysis. Fig. 1 illustrates the fiber distributions and orientations for 10, 20, 30 and 40 wt% fiber reinforced hybrid composites (see Table I for conversion of weight fraction to fiber volume fraction). In the 10 wt% case, Fig. 1a, fiber

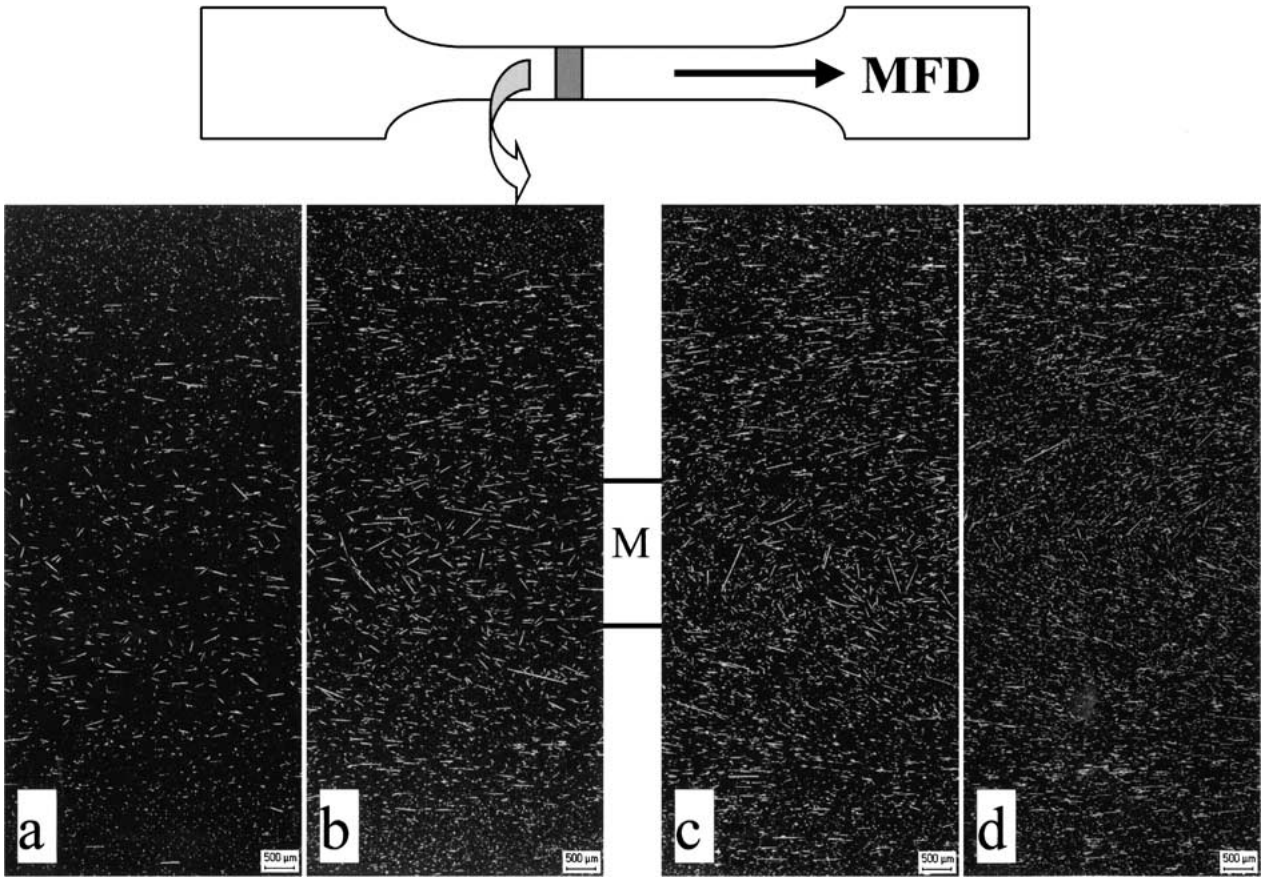

Figure 1 SEM photomicrograph of a polished middle section of rubber toughened nylon 6,6 reinforced with (a) 10 wt%, (b) 20 wt%, (c) 30 wt% and (d) 40 wt% short glass fibers. MFD denotes the mold filling direction and M is the mid layer.

distribution appears sparse but the density of fiber distribution gradually increases as fiber weight fraction increases. A relatively thin skin layer is present in all compositions. Scanning from the surface layer across the in-plane width of a dog-bone specimen it is noted that there is a distinctive skin-core layering morphology as is common in injection molded fiber-reinforced thermoplastics. A thin skin layer shows fibers transverse to the mold filling direction (MFD) whereas fibers near the core are lying on the plane parallel to the MFD. The core region also shows more random alignments on the plane. As fiber concentration increases more fibers are distributed in the core layer wherein increasing alignment of the fibers parallel to the mold filling direction can be observed. The microstructural results are consistent with Friedrich's model [14] whereby fiber orientation increases as a function of fiber volume fraction in injection molded reinforced plastics. It is noted that a middle layer (M) with fibers aligned transverse to the MFD can be seen in 20 and 30 wt% compositions (Fig. 1b and c) whereas the M layer disappears in 40 wt% composition (Fig. 1d).

Fiber orientation is studied using image analysis software and is shown in Fig. 2. The measurement of counts made on in-plane fiber alignment is plotted against the angle between fiber and MFD, excluding the ones lying out of plane. A general trend of counts decreasing with an increase of angle between the fiber alignment and MFD exists in all concentrations. Fig. 3 plots the fiber length distribution as measured in the burnt-off injection molded specimens. According to Karger-Kocsis and Friedrich [15], the average fiber length slightly decreases with an increase in fiber volume fraction. Based on the results given in Fig. 3 the fiber length distribution appears consistent for all compositions. Repeated measurements for all the compositions show that there is no correlation between average fiber length with fiber content. These results are consistent with those reported by Paul and collaborators [7]. The average fiber lengths in the materials studied fall in between 220–260 μm for all compositions. A simple estimation of the critical fiber transfer length based on the Kelly-Tyson model [20] is given by:

$$l_c = \frac{d\sigma_f}{2\tau} \tag{1}$$

where σ_f is fiber strength (=1.5 GPa), τ is interfacial shear strength and is taken to be $\frac{\sigma_m}{2} = \frac{42.71\,\text{MPa}}{2} =$ 21.35 MPa and d is fiber diameter (=17 μm). As a result, $l_c = 0.597$ mm. This value is greater than the average fiber lengths after processing. Clearly, stress transfer from the matrix to the fiber is not optimized in this case and the fibers will be pulled out rather than broken. For weaker interface bond strength, the critical length would only be longer using Equation 1 since τ would be lower. In the discussion that follows, we will show how fibers reduce the fraction of the composite load borne by the matrix and, in so doing, toughening arising from the second-phase rubber particles is curtailed.

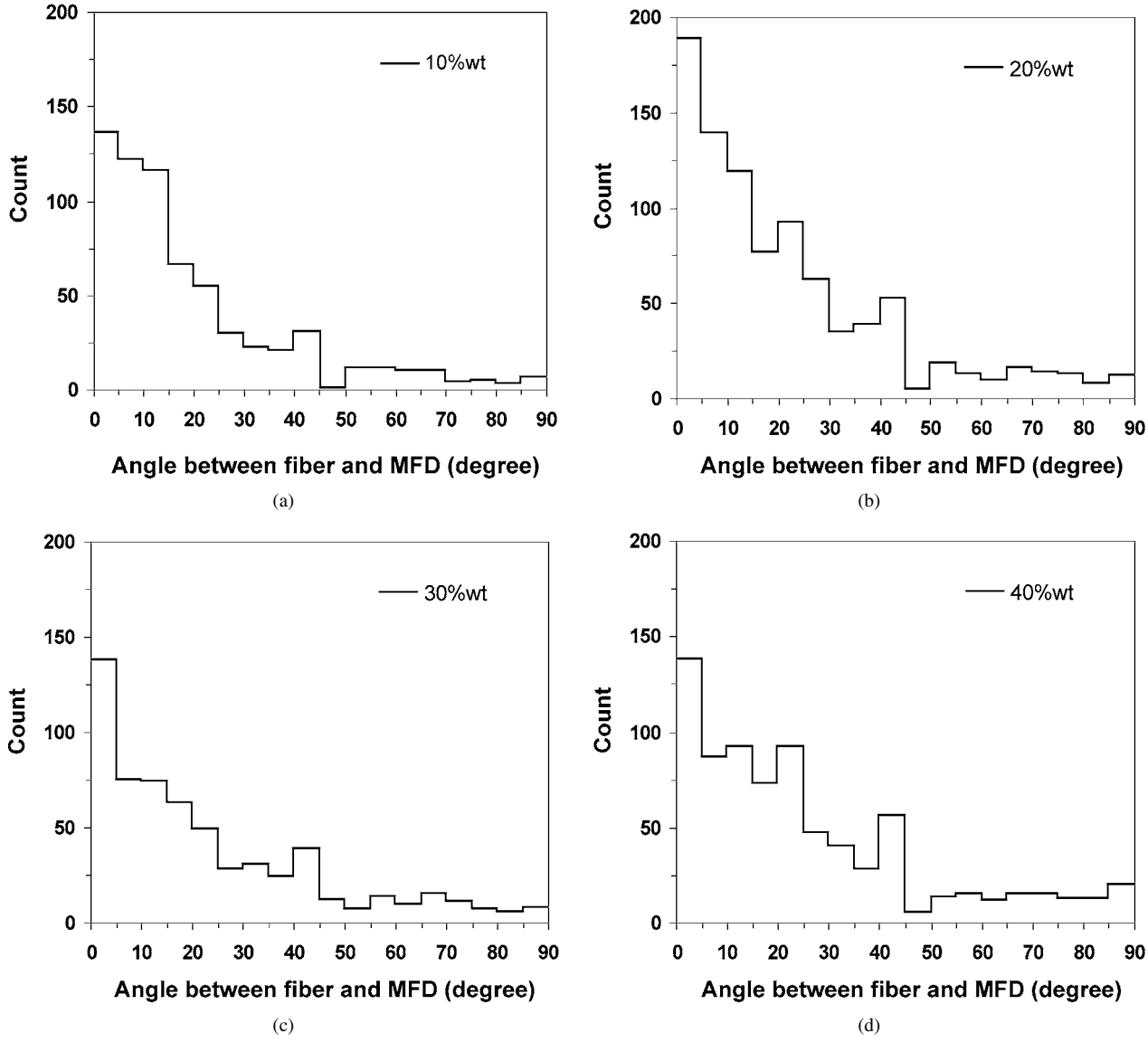

Figure 2 Counts made on in-plane cross-section versus the angle between fiber and MFD on a polished middle section of toughened nylon 6,6 reinforced with (a) 10 wt%, (b) 20 wt%, (c) 30 wt% and (d) 40 wt% short glass fibers.

3.2. Toughening mechanisms

Fig. 4 plots the specific essential work (w_e) and the slope (βw_p) as interpreted in Chapter 20 of Ref. [3], which is indicative of the non-essential plastic work versus the fiber weight fraction. The plot gives very useful information as to how the toughening mechanisms transform from one that is governed by matrix deformation to that governed by fiber-related mechanisms. For the un-reinforced toughened matrix, the specific essential work is comparatively low with a very high value of the specific non-essential plastic work. This suggests the major deformation occurs in the nylon matrix with profuse shear yielding outside the fracture process zone (FPZ). Note that the plastic work outside the FPZ is dependent on specimen geometry and loading configuration [21, 22]. Upon introduction of 10 wt% short glass fibers, there is a pronounced increase in w_e. However, the drop in the slope of non-essential plastic work is more drastic. Since the glass fibers possess a much higher stiffness than the polymer matrix, they will take on a larger proportion of the applied composite stress. Effectively, this means that the matrix loading was shed onto the fibers. Consequently, the overall plastic matrix deformation away from the FPZ is curtailed. The effect of load shedding from the matrix onto the fibers can be demonstrated by recognizing that in a short fiber composite, the average matrix stress σ_{ms} can be estimated by

$$\sigma_{ms} = \frac{\sigma_c - \bar{\sigma}_f v_f}{(1 - v_f)} \tag{2}$$

where σ_c is the composite stress and $\bar{\sigma}_f$ is the average fiber stress and v_f is the fiber volume fraction. In this system, the fiber lengths are less than the critical load transfer length, l_c, as given by Equation 1. Therefore,

$$\bar{\sigma}_f = \frac{\tau l}{d} = \sigma_m \times \frac{s}{2} \tag{3}$$

where s is the fiber aspect ratio. Accordingly, the ratio of σ_{ms}, the matrix stress with fibers to the composite stress ($\approx\sigma_c$) is

$$\frac{\sigma_{ms}}{\sigma_c} = \frac{\sigma_c - \sigma_m s \dfrac{v_f}{2}}{\sigma_c(1 - v_f)} \tag{4}$$

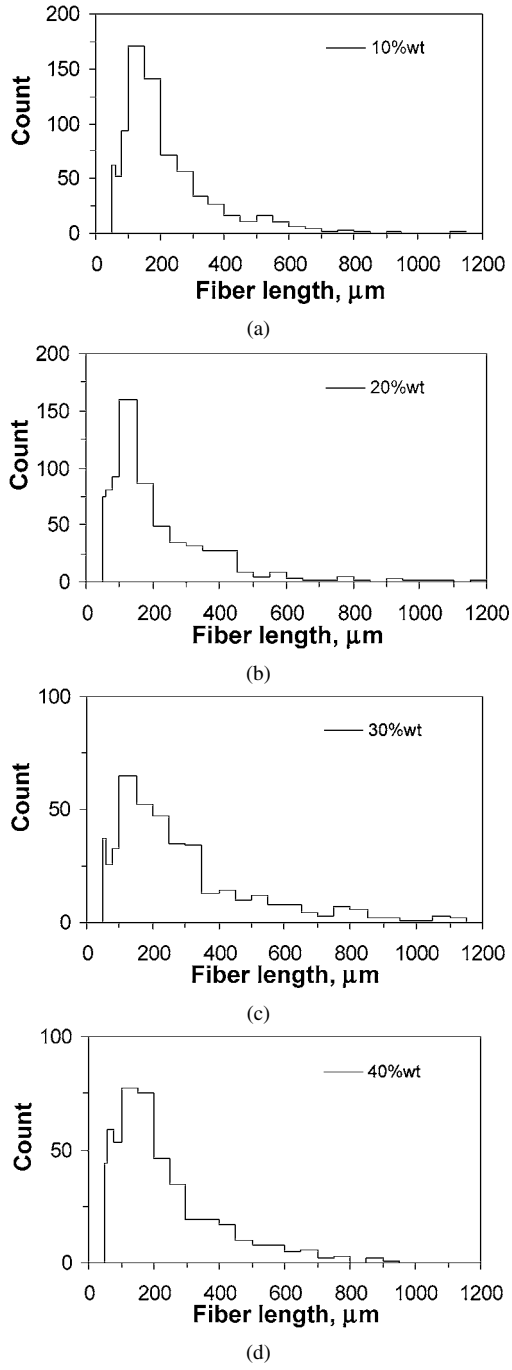

Figure 3 Glass fiber length distributions measured on the fibers extracted from the injection molded bars of (a) 10 wt%, (b) 20 wt%, (c) 30 wt% and (d) 40 wt% short glass fiber reinforced toughened nylon 6,6.

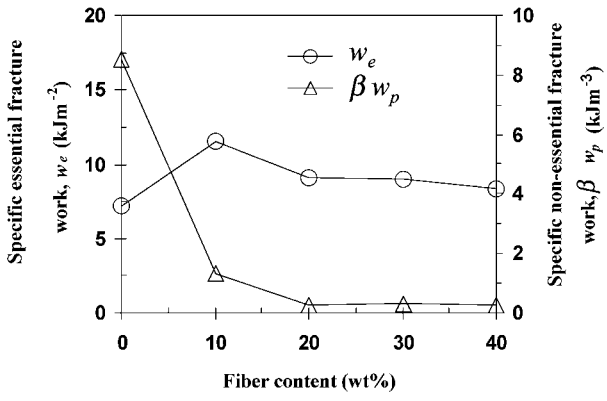

Figure 4 Specific essential and non-essential work of fracture versus fiber weight content.

Substituting the values given in Table II, we could calculate using Equation 4 $\frac{\sigma_{ms}}{\sigma_c} \approx 0.73, 0.57, 0.52, 0.42$ for 10, 20, 30 and 40 wt% fiber reinforced toughened nylon 6,6, respectively. In Equation 2 we have assumed that the fibers are perfectly aligned parallel to the MFD and the applied stress acts on a cross-section containing fibers and matrix as in a uniformly loaded tensile specimen. Hence the fiber orientation effect and the non-uniform crack-tip stress field have been ignored. If we assume the short fibers are 2-D randomly aligned, then the effective length, $\bar{l}$, for reinforcement is given by

$$\bar{l} = \frac{N \int_0^{\pi/2} l \cos\theta \, \mathrm{d}\theta}{N(\pi/2)} = 0.637l, \tag{5}$$

where N is the total number of fiber and θ is the projected angle of fibers from the plane parallel to the MFD, respectively. As a result, Equation 4 can now be modified as follows:

$$\frac{\sigma_{ms}}{\sigma_c} = \frac{\sigma_c - \eta\sigma_m s \dfrac{v_f}{2}}{\sigma_c(1 - v_f)}, \tag{6}$$

where the fiber orientation efficiency factor, $\eta = 0.637$.

From Equation 4 even though the fiber length is smaller than the critical transfer length, the matrix stress could be substantially reduced by as much as 27–58%. Thus, the role of stress shedding in reducing the matrix deformation appears very plausible and may play a key role in the mechanics of fracture in composites containing second phases distributed among the fiber reinforced hybrid materials. Plots of Equations (4) and (6) versus fiber weight fraction are given in Fig. 5. Similar trends are shown as those data obtained for the specific non-essential plastic work in Fig. 4. There appears to be an interesting correlation between the reduction in non-essential plastic work and the reduction in matrix-borne stress. Equation 6, which takes into account the effect of 2-D random orientation, shows a greater resemblance

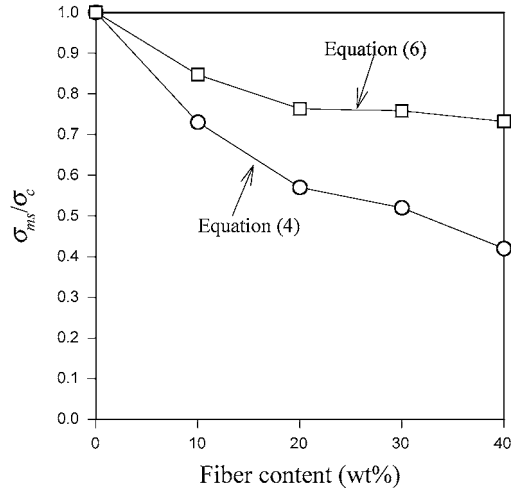

Figure 5 The ratio of the matrix stress to composite stress, σ_{ms}/σ_c, versus fiber weight content. Equation 4 is derived from the assumptions of uniform alignment and uniformly applied load. Equation 6 is derived from the assumption of 2-D random orientation.

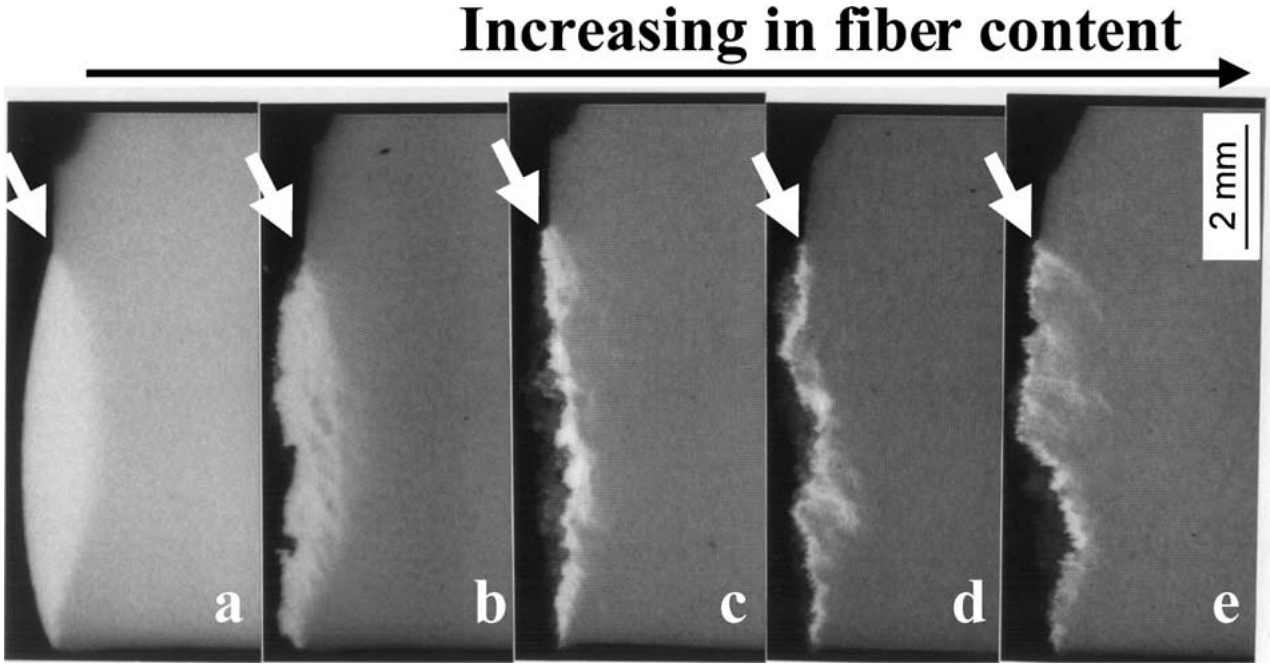

Figure 6 Optical photographs showing the plastic deformation zone beneath the fracture surface. The white arrows on the photographs indicate the onset of crack propagation. (a) un-reinforced toughened nylon 6,6; (b) 10 wt%; (c) 20 wt%; (d) 30 wt%; (e) 40 wt% fiber reinforced toughened nylon 6,6.

of the trend in Fig. 4, particularly towards high fiber content. The reduction in specific non-essential work levels off at higher fiber content. The reduction in matrix stress critically influences the sequence of events upon fracture and decreases the non-essential plastic work during crack growth. We believe this result is interesting and warrants further study on the correlation observed.

One important factor we have ignored is interface bonding. It is believed the inter-facial bonding between the fibers and the matrix containing rubber particles [16] plays an important role in promoting matrix plasticity both in the FPZ and the surrounding plastic/damage zone. Without going through a rigorous crack-tip stress-strain field analysis covering these two zones, we can, for the present purpose, resort to a simple qualitative explanation. A weak interface in a short fiber composite material generally lowers the reinforcing effectiveness of the fibers. A strong interface will be able to impart strength and stiffness to the composite by shedding the load from the matrix to the fibers and the σ_{ms}/σ_c ratio is reduced. When fiber-matrix debonding occurs, which usually happens at the ends of a single fiber where the shear stresses are highest, it can activate local matrix plastic deformation. This effect causes a whitened zone near the crack-tip region. If fiber-matrix debonding does not occur and the triaxial stress (at any point inside these two zones) borne by the matrix is sufficient to activate rubber cavitation, then toughening (in the FPZ) and plastic deformation (outside the FPZ) will occur by matrix shearing between the fibers. We note that inside the crack-tip FPZ, we can have either matrix-dominant or fiber-dominant fracture depending on the fiber volume fraction.

The specific essential fracture work is the total work per unit area of crack growth that is dissipated in the FPZ and required to debond and pull out the fiber as well as to deform and tear the matrix ligament. When the matrix-borne stress is low, such as in high fiber volume systems, the FPZ is dominated by fiber-related mechanisms, namely, fiber debonding, bridging, and pullout. The longer the fiber lengths the greater the fiber pull-out work. Outside the FPZ the size of the plastic/damage zone is, however, small due to the low matrix stress there. For low fiber volume systems ($<10\%$), the dominant failure mechanisms will be rubber cavitation and matrix plastic shear deformation. There will also be some contributions due to fiber-related mechanisms. Fig. 6 compares the damage zones caused by different fiber concentrations. Fig. 6a shows extensive plastic deformation as characteristic of single-edge-notch-bend toughened polymers under quasi-static conditions. Introduction of short glass fibers sheds considerably the composite stress to the fibers hence curtailing the matrix plastic deformation as shown in Fig. 6b. However, the stress-whitened zone is still significant at 10 wt% fibers. This is because, prior to fiber-matrix debonding, there is still sufficient matrix triaxial stress to cavitate the embedded rubber particles and hence matrix plastic deformation is enhanced. An increase in fiber content generates tortuous fracture paths that are indicative of pervasive crack deflections at fiber-matrix interface and near fiber-ends. The stress-whitened zone is also drastically diminished (Fig. 6c, d and e) due to the load shedding mechanism as discussed earlier.

Examination of sub-critically loaded cracks also confirms the above results. Figs. 7 and 8 present photomicrographs of the sub-critical crack-tip deformation obtained from ROM and TOM, respectively. Clearly, the un-reinforced matrix produces profuse ligament yielding with a large whitened zone whereas the fiber-containing matrices show crack deflection with reduced matrix plastic deformation outside the FPZ. At 10 wt% considerable damage/plastic deformation is still being

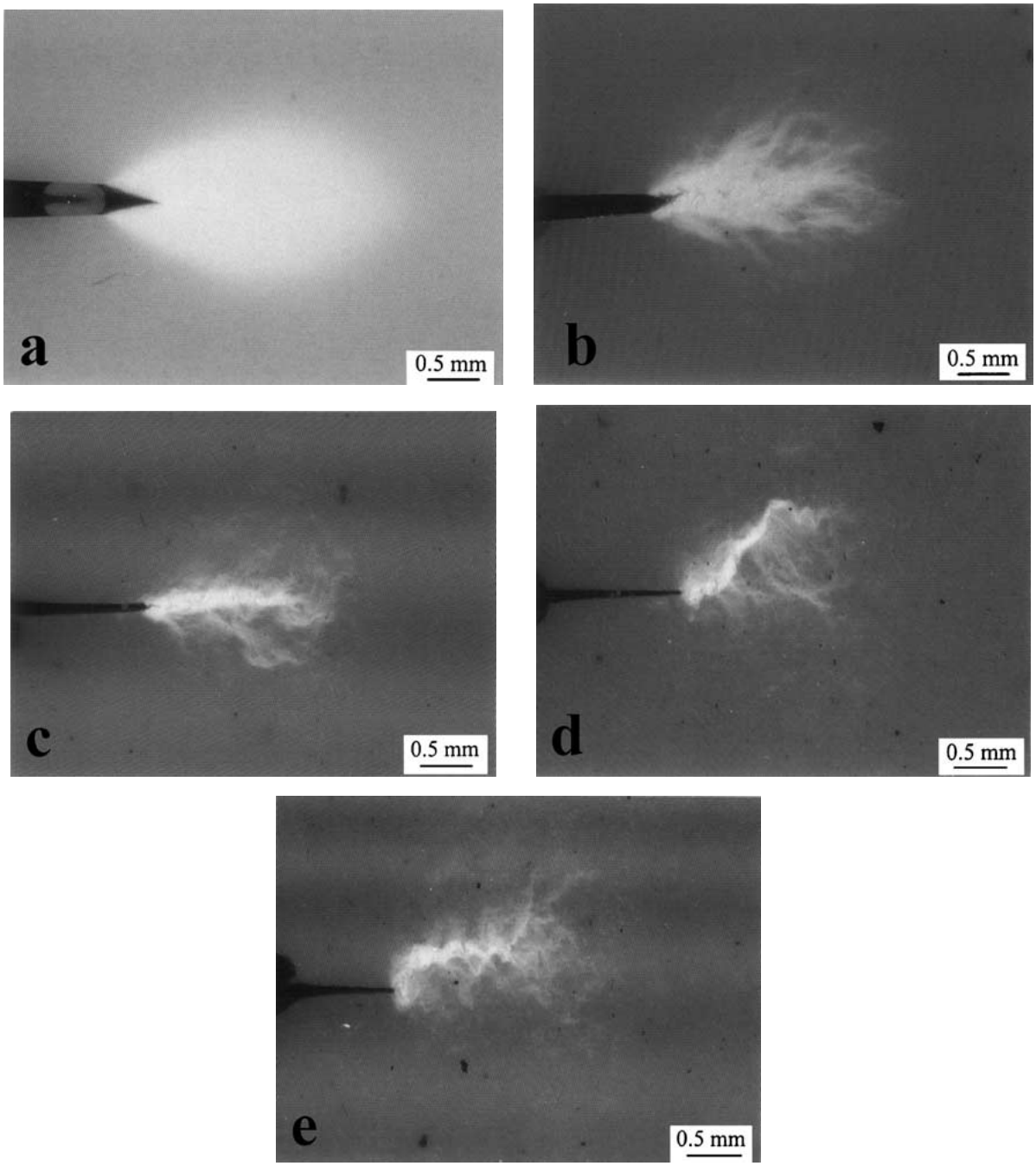

Figure 7 ROM micrographs of sub-critically loaded cracks in SEDN-4PB technique for (a) un-reinforced toughened nylon 6,6, (b) 10 wt%, (c) 20 wt%, (d) 30 wt% and (e) 40 wt% fiber reinforced toughened nylon 6,6.

observed near the crack-tip. With higher fiber content (20, 30 and 40 wt%), a larger proportion of the applied stress will be shed onto the fibers, which results in extensive fiber-related toughening with little matrix plastic deformation. The tortuous crack paths are consistent with what we observed in Fig. 6c–e. These twisted crack paths are derived from the extensive fiber-end and fiber-matrix debonding.

Fig. 9 compares the un-deformed and fracture subsurfaces of fiber-containing toughened nylon 6,6 under BEI in SEM. The rubbery phase is stained with OsO_4, which gives a much stronger imaging of back-scattered electrons. The rubbery phase appears bright whereas the nylon phase appears dark in these micrographs. Close examination of the fiber-end region shows extensive distortion of rubber particles. The distorted rubbery phase is indicative of severe shear deformation at the fiber ends. Shiao *et al.* [23] modeled the contribution of fiber-end plasticity to increasing fracture toughness for brittle composites using the critical distance, L_c, concept as follows:

$$K_c = \left(\frac{\varepsilon_f^* \sigma_c E_c L_c}{C_1 C_2} \right)^{1/2} \tag{7}$$

where K_c is the critical stress intensity factor of the composite, ε_f^* is the critical strain as obtained from the fracture strain of the composite [23], E_c is the composite modulus, C_1 and C_2 are constants. It was suggested that fiber-end debonding could generate stress concentrations embrittling the matrix material. It could

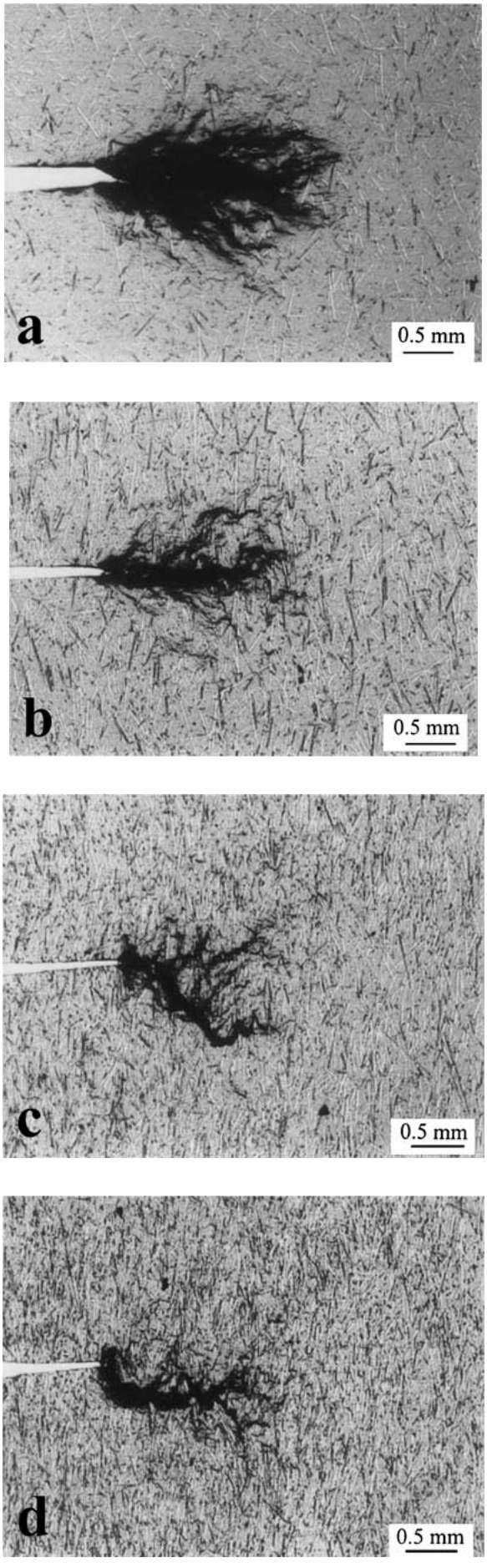

Figure 8 TOM micrographs of thin sections for (a) 10 wt%, (b) 20 wt%, (c) 30 wt% and (d) 40 wt% fiber reinforced toughened nylon 6,6. Note that fiber distribution density increases near the crack front from (a) to (d).

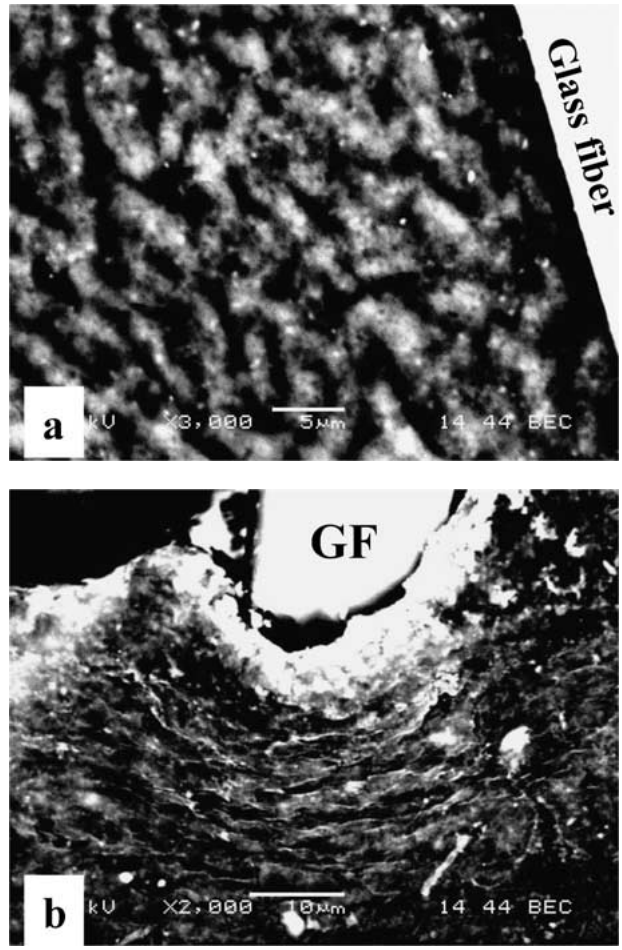

Figure 9 SEM/BEI photomicrographs of 20 wt% short glass fiber reinforced toughened nylon 6,6 for (a) a non-deformed specimen and (b) a fractured subsurface. The dark phase is nylon and the light phase is EPDM rubber.

also enhance matrix toughness when a critical fiber-end distance is reached. This critical distance was to allow stress field overlapping between fiber ends [23] and thereby matrix plasticity is enhanced. In the results we presented, we observed highly localized plastic deformation in front of an advancing crack. Obviously, fiber debonding and pullout occurred well in advance of matrix material remote from the crack-tip being able to deform profusely. It would be necessary to establish the criterion of fiber-end debonding prior to taking full advantage of fiber-end plasticity for toughening.

The optimal conditions for both fiber- and rubber-toughening to be cooperative are not very clear. It appears from Fig. 4, however, that the largest w_e is obtained at 10 wt% fiber content. This point was never discussed and simulated in most short fiber composite studies to our best knowledge. Too high a fiber content will suppress the matrix toughening and will only retain those fiber-related toughness contributions. Vice versa, too low a fiber content will be dominated by matrix toughening as activated by rubber cavitation. Also, the fiber-matrix adhesion will control the debonding mechanism and fiber-end induced plasticity. Further studies should focus on the effect of interfacial adhesion on fiber toughening. In addition, it is necessary to perform a full field stress analysis of the crack-tip region including both the FPZ and the surrounding plastic zone (in the presence of both fiber inclusions and rubber

particulates) in order to determine the stresses borne by the matrix material and the fiber. Analytical treatments of toughness taking only the effective properties of the rubber-toughened matrix in which the short fibers are dispersed, as if this were a pseudo two-phase material, will be deficient because they ignore the matrix toughness contribution activated by rubber cavitation.

4. Conclusions

The fracture toughness of short glass fiber reinforced toughened nylon 6,6 was assessed using the EWF technique and the microstructures and toughening behavior were characterized using both electron and optical microscopic techniques. According to the EWF analysis and the microscopic observations, the following conclusions were made.

1. The inclusions of short glass fibers in the rubber-toughened polymers not only provided a stiffening effect but also a toughening influence.
2. Rubber toughening and fiber toughening exhibited competitive behavior. When matrix stress was substantially reduced by load-shedding onto the fibers, rubber toughening mechanisms were curtailed.
3. Fiber-related fracture processes governed in high fiber volume fractions. The fiber pullout work contributed considerably to the specific essential work of fracture.
4. Fiber-end plasticity was evident under microscopic examination. It was necessary to establish the critical debonding criterion before being able to take full advantage of fiber-end plasticity.

Acknowledgments

The authors would like to thank the Nanyang Technological University for providing the financial support for this project under research grant RG 21/00. YWM is also supported by the Australian Research Council on fiber-toughened blends.

References

1. C. B. BUCKNALL, in "Toughened Plastics" (Applied Science Publishers, London, 1977).
2. R. A. PEARSON, H. J. SUE and A. F. YEE (eds.), "Toughening of Plastics: Advances in Modeling and Experiments," ACS Symposium Series 759 (American Chemical Society, Washington D. C., 2000).
3. D. R. PAUL and C. B. BUCKNALL (eds.), "Polymer Blends, Vol. 2: Performance" (Wiley-Interscience, New York, 2000).
4. S. V. NAIR, M. L. SHIAO and P. D. GARRETT, *J. Mater. Sci.* **27** (1992) 1085.
5. T. J. PECORNI and R. W. HERTZBERG, *Polym. Comp.* **15** (1994) 173.
6. S. C. WONG and Y. W. MAI, *Polym. Eng. Sci*. **39** (1999) 356.
7. D. M. LAURA, H. KESKKULA, J. W. BARLOW and D. R. PAUL, *Polymer* **41** (2000) 7165.
8. *Idem.*, *ibid*. **42** (2001) 6161.
9. J. KARGER-KOCSIS, *J. Polym. Eng*. **12** (1993) 77.
10. H. ZHANG and L. A. BERGLUND, *Polym. Eng. Sci*. **33** (1993) 100.
11. D. E. MOUZAKIS, F. STRICKER, MÜLHAUPT and J. KARGER-KOCSIS, *J. Mater. Sci.* **33** (1998) 2551.
12. J. LEE and A. F. YEE, *ibid.* **36** (2001) 7.
13. S. V. NAIR, S.-C. WONG and L. A. GOETTLER, *ibid.* **32** (1997) 5335.
14. K. FRIEDRICH, *Comp. Sci. Technol*. **22** (1985) 43.
15. J. KARGER-KOCSIS and K. FRIEDRICH, *ibid.* **32** (1988) 293.
16. S. V. NAIR, A. SUBRAMANIAM and L. A. GOETTLER, *J. Mater. Sci.* **32** (1997) 5347.
17. H. J. SUE and A. F. YEE, *J. Mater. Sci.* **28** (1993) 2975.
18. M. T. TAKEMORI and A. F. YEE, in "Impact Fracture of Polymers—Materials Science and Testing Techniques," edited by K. Takahashi and A. F. Yee (Kyushu University, Fukuoka-shi, Japan, 1992) p. 331.
19. J. S. WU, C. M. CHAN and Y. W. MAI, in "Polymer Blends and Alloys," edited by G. O. Shonaike and G. P. Simon (Marcel Dekker, New York, 1999) ch. 18, p. 505.
20. A. KELLY and W. R. TYSON, *J. Mech. Phys. Solids*. **13** (1965) 329.
21. Y. W. MAI and B. COTTERELL, *Int. J. Fract*. **32** (1986) 105.
22. J. S. WU and Y. W. MAI, *Polym. Eng. Sci*. **36** (1996) 2275.
23. M. L. SHIAO, S. V. NAIR, P. D. GARRETT and R. E. POLLARD, *Polymer* **35** (1994) 306.

Received 14 August 2001
and accepted 27 February 2002